Interfaces for High-Speed Fiber-Optic Links: Analysis and Experiment

Afshin S. Daryoush, *Senior Member, IEEE*, Edward Ackerman, *Member, IEEE*, Niranjan R. Samant, *Student Member, IEEE*, Stephen Wanuga, *Senior Member, IEEE*, and Dumrong Kasemset, *Member, IEEE*

Abstract—**An analysis of directly and externally modulated fiberoptic links is presented here. The theoretical analysis is based on the signal flow diagram of the interface circuits to the laser diode, Mach–Zehnder electro-optic modulator, and p-i-n photodiode. System parameters such as gain, noise figure, two-tone intermodulation distortion, and spurious free and compression dynamic range are expressed as a function of frequency and operating point of the laser and external modulator. Two directly and externally modulated fiber-optic links were designed and fabricated to verify the analytical models. The direct modulation FO link was developed at the *Ku*-band (11.6–12.4 GHz), whereas the external modulation link was at *L*-band (875–925 MHz). Spurious-free dynamic ranges of 95.8 dB·Hz$^{2/3}$ and 113 dB·Hz$^{2/3}$, respectively, were achieved, the best reported to date for these frequency bands. The predictions based on the analytical models match the measured results very well.**

Introduction

HIGH-SPEED fiber-optic links are envisioned as playing a major role in many microwave circuits and systems [1]. Some potential applications include antenna remoting and distribution networks [2], delay lines [3], and optical control of microwave devices [4]. Accurate modeling of the FO link performance will aid the system designer in evaluating the suitability of the viable architectures to specific applications. Most of the fiber-optic links designed for microwave applications are relatively short to medium length (up to 1 km) and employ intensity detection techniques. The intensity modulation of light is realized via either direct modulation of a semiconductor laser diode or external modulation of laser light by taking advantage of the interaction of light with matter. Of the various external modulation schemes, the most common presently use travelling-wave or lumped-element Mach–Zehnder modulators that operate using the electro-optic properties of $LiNbO_3$ [5] or GaAs [6].

Until now, there has not been a full analytical model for direct and external modulation fiber-optic links that presents the important link parameters—such as gain, noise figure, two-tone intermodulation distortion, compression and spurious free dynamic range—in a language accessible to the microwave engineer. Even though attempts to explain the link performance in terms of equivalent circuit parameters have been made [7]–[11], these models suffer from inaccurate prediction of broadband FO link performance. Some even have incorrect physical circuit models with unreasonable component values. Thus, the goal of this paper is to present the analytical models necessary to predict FO link performance. Furthermore, analytical models are used as guidelines to develop low loss, high dynamic range FO links. The experimental results are compared to the analytical models' predictions to verify the models.

Manuscript received March 29, 1991; revised August 14, 1991. This work was supported by GE Aerospace Division, NASA Lewis Research Center, and the Ben Franklin Partnership of the State of Pennsylvania.

A. S. Daryoush and N. R. Samant are with the Center for Microwave-Lightwave Engineering, Drexel University, Philadelphia, PA 19104.

E. Ackerman, S. Wanuga, and D. Kasemset are with the GE Electronics Laboratory, Syracuse, NY 13221.

IEEE Log Number 9103519.

Device Characterization and Modeling

An essential part of low-loss, high dynamic range FO link design is the development of reactively matched interface circuits, which are only realizable when the transducer characteristics at microwave frequencies are known. Design steps involve the characterization and modeling of the semiconductor laser diode and electro-optic modulator as the microwave/optical transducer portions of the two types of optical transmitters. By contrast, an impedance-matched p-i-n photodiode constitutes the optical/microwave transducer in the optical receiver for both architectures. Standard TRL de-embedding techniques are adequate for extracting the intrinsic transducer's impedance at microwave frequencies from the measured impedance of the device in its test fixture. The de-embedded impedance is then fitted to an equivalent circuit model over a broad bandwidth by the use of a realistic physical model.

The conceptual block diagram of the direct modulation optical transmitter at microwave frequencies, Fig. 1, shows an impedance matching circuit with the laser equivalent circuit model and the corresponding signal flow diagram. The circuit elements are based on the physical parameters of the laser and their values are obtained from the TRL de-embedding of the intrinsic laser impedance. The goal of the matching network is to effectively transfer current at the design frequency band from the 50 Ω

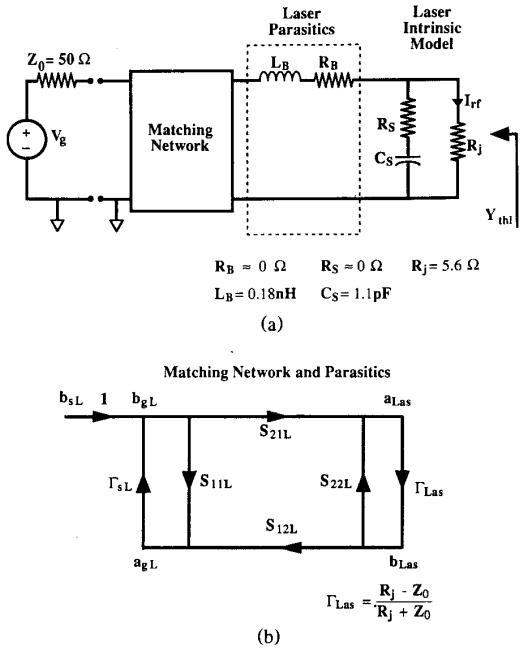

Fig. 1. Semiconductor laser diode as the microwave/optical interface. (a) Intrinsic and extrinsic equivalent circuit model with values for a *Ku*-band link. (b) Signal flow diagram model.

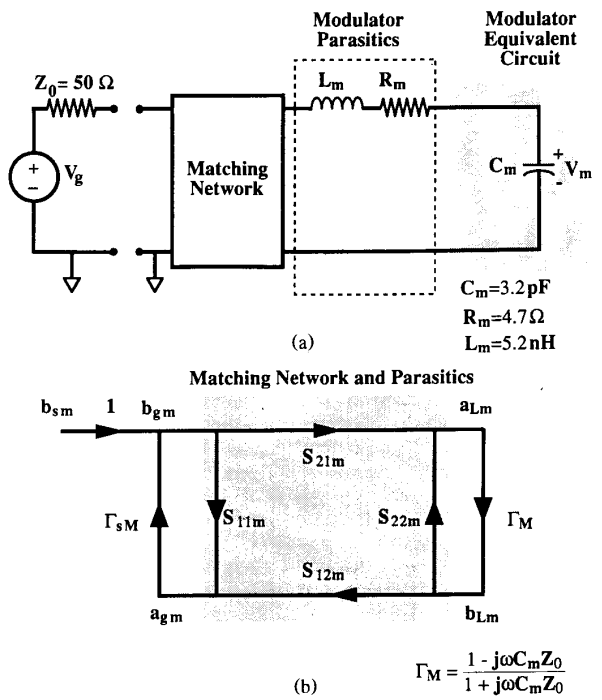

Fig. 2. Mach–Zehnder lumped-element external electro-optic modulator as the microwave/optical interface. (a) Intrinsic and extrinsic equivalent circuit model with values for an *L*-band link. (b) Signal flow diagram model.

system input to the junction of the laser diode, denoted by the current I_{rf} passing through the forward-biased p-n junction resistance R_j. Since R_j is less than 10 Ω, the matching network is effectively a 50 Ω to approximately 10 Ω impedance transformer. The minimum reflection coefficient attainable using reactive matching techniques will be limited by the quality factor of the laser and the percentage bandwidth over which impedance-matching is performed; for example, the theoretical limit for minimum return loss achieved over a 2–4 GHz bandwidth for a buried hetero-junction semiconductor laser (such as Ortel's SL1000H) is −14 dB.

The optical transmitter module of an externally modulated FO link, Fig. 2, shows the equivalent circuit of a lumped-element Mach–Zehnder modulator and the signal flow diagram of the transmitter. The impedance matching network in the Mach–Zehnder modulator transforms the input signal so that at the design frequency band maximum voltage V_m is obtained across the capacitor C_m. The lumped series resistance R_m, with typical values of about 5 to 6 Ω, forms the effective load resistance. The limitation imposed on the impedance matching network is by the quality factor of the external modulator determined by C_m and R_m. For example, the lumped-element $LiNbO_3$ Mach–Zehnder modulator used in the 875–925 MHz link has a minimum return loss of −11.6 dB across the band. Using reactive matching networks results in satisfactory matching.

A block diagram of the optical receiver module, Fig. 3, shows a p-i-n photodiode equivalent circuit model and the

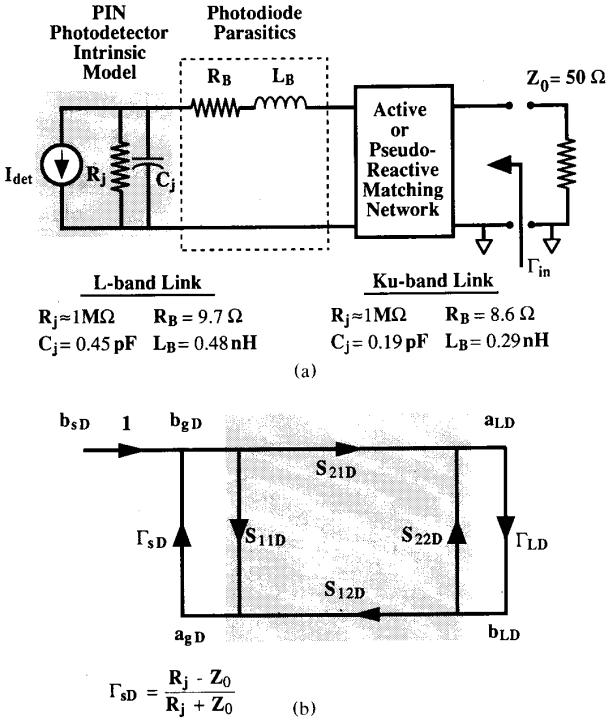

Fig. 3. p-i-n photodiode as the optical/microwave interface. (a) Intrinsic and extrinsic equivalent circuit model. (b) Signal flow diagram model.

receiver matching network. The goal of the matching circuit is to effectively transform the RF photocurrent I_{det} to the 50 Ω load. Ideally, an impedance matching network for the receiver would entail the matching of the photodiode's high shunt junction resistance R_j—typically 1 MΩ—to the output of the FO link, which is a 50 Ω system. The quality factor of the photodiode is extremely high if parasitics are small. However, the de-embedding and equivalent circuit modeling of the photodetectors reveals that the parasitic series resistance dominates over the reverse-biased p-n junction resistance at microwave frequencies. This series resistance, R_B, therefore dictates a lower overall Q-factor. Thus it is the series resistance R_B that is transformed to 50 Ω in the detector's impedance matching network. For example, in the case of the InGaAs p-i-n photodiode used in the 11.6–12.4 GHz link, de-embedding and equivalent circuit modeling yielded R_j of approximately 1 MΩ, $C_D = 0.19$ pF, and a parasitic series resistance $R_B = 8.6$ Ω. Across the 11–13 GHz band, therefore, the best achievable return loss is −20.2 dB. However, over broad bandwidths active matching techniques using MESFET's leads to improved return loss for the optical receiver.

Directly Modulated FO Links

Gain Analysis

The gain of a fiber-optic link can be calculated in terms of microwave scattering parameters using the signal flow diagram (SFD) technique. The transducer gains of the optical transmitter and optical receiver are derived separately and then combined to yield the gain of the complete link. When a directly modulated semiconductor laser diode is employed in the optical transmitter, the SFD is obtained by considering the forward-bias junction resistance of the laser diode to be the port two termination Γ_{Las} of a two-port network (represented by $[S_L]$) consisting of the microwave impedance-matching circuit and other device parameters of the laser. Fig. 1 shows the schematic diagram and SFD for the transmitter in a direct modulation link. The output power of a fiber-optic link depends on the amplitude of photocurrent, I_{det}, generated in the detector, which is in turn proportional to the RF current, I_{rf}, through the laser diode's active region. This RF current is expressed as

$$I_{\text{rf}} = \sqrt{Y_0}\,(a_{\text{Las}} - b_{\text{Las}}), \tag{1}$$

where a_{Las} and b_{Las} are of the normalized input and output powers, respectively, at the laser junction resistance, and Y_0 is the characteristic admittance of the transmitter input (i.e., 20 mS for a standard 50 Ω system). From the SFD it is clear that

$$a_{\text{Las}} = \frac{I_{\text{rf}}^{+}}{\sqrt{Y_0}} = \frac{b_{SL}S_{21L}}{(1 - S_{22L}\Gamma_{\text{Las}})} \quad \text{and}$$

$$b_{\text{Las}} = \frac{I_{\text{rf}}}{\sqrt{Y_0}} = \frac{b_{SL}S_{21L}\Gamma_{\text{Las}}}{(1 - S_{22L}\Gamma_{\text{Las}})}. \tag{2}$$

By definition, the power delivered to the laser junction is the difference between the incident and reflected powers, i.e.:

$$P_{\text{out},Tx} = |a_{\text{Las}}|^2 - |b_{\text{Las}}|^2 = \frac{|b_{sL}|^2 \times |S_{21L}|^2 \times |1 - \Gamma_{\text{Las}}|^2}{|1 - S_{22L}\Gamma_{\text{Las}}|^2}. \tag{3}$$

Hence the transducer gain of the directly modulated laser-based optical transmitter is

$$G_{Tx} = \frac{P_{\text{out},Tx}}{|b_{sL}|^2} = \frac{|S_{21L}|^2 \times |1 - \Gamma_{\text{Las}}|^2}{|1 - S_{22L}\Gamma_{\text{Las}}|^2}. \tag{4}$$

The link current transfer function, H_L, is defined as the ratio of detector current I_{det} to RF current I_{rf} across the laser and is given by

$$\left(\frac{P_{\text{in},RX}}{P_{\text{out},TX}}\right) = \frac{|I_{\text{det}}|^2}{|I_{\text{rf}}|^2} = |H_L|^2$$

$$= (\eta_L K_L L K_D \eta_D)^2 |H_{\text{Las}}(f, I_b)|^2 |H_{\text{det}}(f, V_b)|^2, \tag{5}$$

where η_L is the laser diode external quantum efficiency, η_D is the photodetector responsivity, L is the optical attenuation in the fiber, and K_L, K_D are the laser-to-fiber and fiber-to-detector coupling efficiencies, respectively. $|H_{\text{Las}}(f, I_b)|^2$ and $|H_{\text{det}}(f, V_D)|^2$ are the frequency transfer characteristics of the laser and photodetector, respectively, for the given operating biases. For links operating well below the observable 3-dB bandwidth in the laser and detector frequency responses, these two terms are both approximately unity.

When a reverse-biased p-i-n photodiode is employed in the optical receiver, the SFD is obtained by considering the junction resistance of the diode to be the source termination Γ_{sD} of a two-port network (represented by $[S_D]$) consisting of the other device parameters of the photodetector and the microwave impedance-matching circuit. Fig. 3 shows the schematic diagram and SFD for the optical receiver. The output microwave power is derived from the SFD and from the square root of the incident and reflected detector powers (a_{LD} and b_{LD}, respectively) as follows:

$$P_{\text{out}} = |a_{LD}|^2 - |b_{LD}|^2 = |a_{LD}|^2 = \frac{|b_{sD}|^2 \times |S_{21D}|^2}{|1 - S_{11D}\Gamma_{sD}|^2}, \tag{6}$$

since $b_{LD} = 0$. Therefore,

$$G_{Rx} = \frac{P_{\text{out}}}{|b_{sD}|^2} = \frac{|S_{21D}|^2}{|1 - S_{11D}\Gamma_D|^2}. \tag{7}$$

The transducer gain of the direct modulation link is thus obtained from the optical transmitter and receiver gains

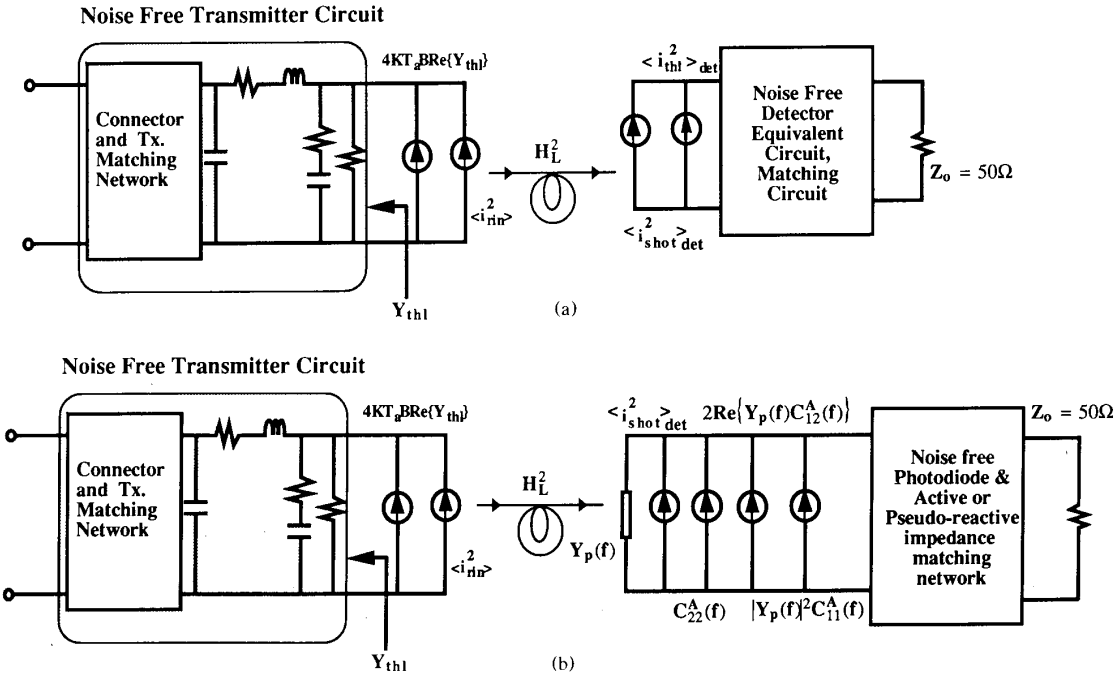

Fig. 4. Schematic representation of noise sources in a directly modulated FO link. (a) With a reactively matched receiver. (b) With an actively matched receiver.

and the square of the link current transfer function; i.e.,

$$G = \frac{P_{\text{out},Rx}}{P_{\text{av},Tx}} = G_{Tx} \cdot H_L^2 \cdot G_{Rx}$$

$$= \frac{|S_{21L}|^2 |S_{21D}|^2 |1 - \Gamma_{\text{Las}}|^2 (\eta_L K_L L K_D \eta_D)^2}{|1 - \Gamma_{\text{Las}} S_{22L}|^2 |1 - \Gamma_{sD} S_{11D}|^2}. \quad (8)$$

Noise Analysis

Three categories of noise sources, shown in Fig. 4, contribute to the total noise powers in the directly modulated FO link, viz. thermal, shot, and relative intensity noise of laser. The various noise sources of the link are derived as follows:

The thermal noise powers of the transmitter and receiver are calculated using the Nyquist theorem [12] by assuming that each of the individual noise sources in any circuit can be represented by an equivalent noise power at the input or output of the circuit, provided the individual noise sources are uncorrelated. By representing the noise power in this fashion the rest of the circuit can be considered to be noise-free. As shown in Fig. 4, an equivalent thermal noise current source is obtained from the total conductance, $\text{Re}\{Y_{\text{thl}}\}$, of the transmitter circuit as seen from the transmitter output. Using the transfer function of the link from the transmitter output to the output of the receiver, the power output of the transmitter thermal noise is obtained as

$$N_{\text{thtx}} = 4kT_a B (\eta_L K_L L K_D \eta_D)^2 \,\text{Re}\{Y_{\text{thl}}\} \frac{|S_{21D}|^2}{|1 - \Gamma_{sD} S_{11D}|^2} Z_0, \quad (9)$$

where B is the resolution bandwidth of the receiver, k is Boltzmann's constant, T_a is the ambient temperature, and Z_0 is the impedance of the output termination (50 Ω).

A major noise source in direct modulation FO links is the semiconductor laser's relative intensity noise (RIN), which arises from the statistical fluctuations of the photon and electron generation rates within the laser. The RIN, which is a function of frequency and bias current, can be calculated from the laser's physical parameters [13]. This RIN is then represented as a current source at the transmitter output whose amplitude is dependent on both frequency (f) and laser dc bias current (I_b). Noise power at the output of the direct modulation link due to laser RIN is calculated as

$$N_{\text{RIN}} = \text{RIN}(f, I_b)(I_b - I_{\text{th}})^2 (\eta_L K_L L K_D \eta_D)^2 \cdot \frac{|S_{21D}|^2}{|1 - \Gamma_{sD} S_{11D}|^2} B Z_0, \quad (10)$$

where I_{th} is the laser threshold current.

The shot noise of the photodiode, like the laser's RIN, makes a major contribution to the total noise output of the link. The total shot noise power in terms of the dc

current detected by the photodiode and the photodiode's dark current (I_d) is given as

$$N_{\text{shot}} = 2e\left[(I_b - I_{\text{th}})(\eta_L K_L L K_D \eta_D) + I_d\right] \cdot B \frac{|S_{21D}|^2}{|1 - \Gamma_{sD} S_{11D}|^2} Z_0, \quad (11)$$

where e is the electronic charge.

The thermal noise of the reactively matched detector makes a negligible contribution to the total link noise output power; it can be calculated as

$$N_{\text{thrx}} = 2kT_a B\left(1 - |\Gamma_{\text{in}}|^2\right), \quad (12)$$

where Γ_{in} is the reflection coefficient looking into the impedance-matched photodetector circuit from its output.

The total noise power at the output of the detector is the sum of all these individual noise powers,

$$N_{\text{out}} = N_{\text{RIN}} + N_{\text{shot}} + N_{\text{thtx}} + N_{\text{thrx}} = N_{\text{RIN}} + N_{\text{shot}} + N_{\text{th}}. \quad (13)$$

The noise analysis with active matching circuit (shown in Fig. 4b) in the receiver circuit is complicated, due to the fact that the noise sources of the active elements are correlated and cannot be added individually. The correlation matrix in the A-representation, for a MESFET, is as follows [14]:

$$C_{11}^A = 2kT_a \cdot R_n \quad (14)$$

$$C_{22}^A = 2kT_a \cdot R_n \cdot |Y_{\text{opt}}|^2 \quad (15)$$

$$C_{21}^A = 2kT_a\left[0.5(F_{\text{min}} - 1) - R_n \cdot Y_{\text{opt}}\right] \quad (16)$$

$$C_{12}^A = C_{21}^{A*} \quad (17)$$

where F_{min} is the minimum noise figure of the MESFET; R_n is the equivalent noise resistance; and Y_{opt} is the optimum source admittance. C_{11}^A and C_{22}^A are the autocorrelations of the noise voltage and noise current source, respectively, and C_{21}^A is the correlation between the voltage and current source. For the MESFET, we can define an equivalent noise current at the input of the receiver in terms of an autocorrelation spectrum of the equivalent noise current as

$$C^I(f) = C_{22}^A(f) + 2\,\text{Re}\left\{Y_p(f) C_{12}^A(f)\right\} + |Y_p(f)|^2 C_{11}^A(f), \quad (18)$$

where $Y_p(f)$ is the input admittance of the MESFET. The noise power due to the FET at the output of the detector is given by

$$N_{\text{FET}} = C^I(f) \cdot B \cdot \frac{|S_{21D}|^2}{|1 - \Gamma_{sD} S_{11D}|^2} Z_0. \quad (19)$$

The thermal noise of the transmitter circuitry N_{thtx}, the laser's RIN noise power N_{RIN} and the shot noise of the photodiode N_{shot} are as given by (9)–(11). The link thermal noise due to the detector and its matching circuitry, not considering that of the MESFET, is negligible and is not considered here. Thus the total noise output of the link is given as

$$N_{\text{out}} = N_{\text{thtx}} + N_{\text{RIN}} + N_{\text{shot}} + N_{\text{FET}}. \quad (20)$$

Since the thermal noise source at the input of the link is expressed as $N_{\text{in}} = kT_a B$, the noise figure of the fiber-optic link now can be defined as

$$NF_{\text{Link}} \equiv \frac{(SNR)_{\text{in}}}{(SNR)_{\text{out}}} = \frac{P_{\text{in}} * N_{\text{out}}}{P_{\text{out}} * N_{\text{in}}} = \frac{1}{G_{\text{Link}}} * \frac{N_{\text{out}}}{N_{\text{in}}}. \quad (21)$$

Distortion Analysis

The distortion characteristics in a direct modulation link are analyzed with respect to the current modulation index m of the laser which is given as $m = I_{\text{rf}}/(I_b - I_{\text{th}})$. The term IMD/C is defined as the power ratio between the optical third order intermodulation product and the fundamental of the optical signal. The total optical power out of the laser for a two tone input signal is given as [15], [16]:

$$P(t) = \frac{P_0}{I_0(a_1) I_0(a_2)} \Bigg[I_0(a_1) I_0(a_2) + 2 I_0(a_2) \sum_{k=1}^{\infty} I_k(a_1) \cosh(\omega_1 t + \theta_1) + 2 I_0(a_1) \sum_{n=1}^{\infty} I_n(a_2) \cosn(\omega_2 t + \theta_2) + 4 \sum_{k=1}^{\infty} I_k(a_1) \cosh(\omega_1 t + \theta_1) \cdot \sum_{n=1}^{\infty} I_n(a_2) \cosn(\omega_2 t + \theta_2) \Bigg] \quad (22)$$

where $I_x(a_i)$ are modified Bessel functions of the xth order and a_i, for $i = 1,2$, can be obtained from the following equation:

$$m_i = a_i \sqrt{\left(\frac{\omega_i^2}{\omega_0^2} - \phi(a_i)\right)^2 + \omega_i^2 \tau_p^2 \left(\frac{1}{\omega_0^2 \tau_p \tau_s} + 1\right)^2} \quad (23)$$

where, for $i = 1,2$: m_i is the optical modulation index; $\omega_i = 2\pi f_i$; f_i is the input signal frequency; $\omega_0 = 2\pi f_0$; f_0 is the relaxation oscillation frequency; τ_p is the photon lifetime in the cavity; τ_s is the spontaneous emission lifetime; τ_p and τ_s are calculated from the laser's physical parameters [16]. The term $\phi(a_i)$ is defined as

$$\phi(a_i) = \frac{2 I_1(a_i)}{a_i I_0(a_i)}. \quad (24)$$

From the laser light output expression we obtain the optical power out of the laser at the fundamental frequency and at the third-order intermodulation optical

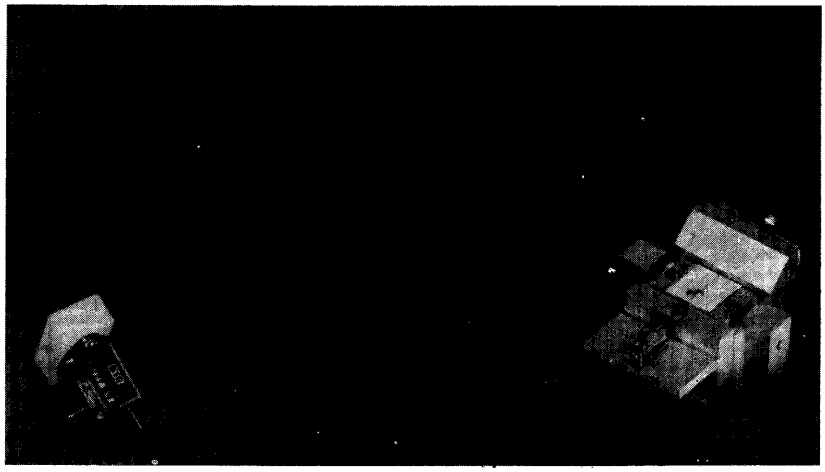

Fig. 5. Direct modulation fiber-optic link optimized for operation at 12 GHz.

power as

$$P_{\omega_1} = \frac{2P_0 I_1(a_1)}{I_0(a_1)} \cos(\omega_1 t), \tag{25}$$

$$P_{2\omega_2-\omega_1} = \frac{2P_0 I_2(a_2) I_1(a_1)}{I_0(a_2) I_0(a_1)} \cos[(2\omega_2 - \omega_1)t]. \tag{26}$$

Thus we obtain IMD/C for small signals as

$$\frac{\text{IMD}}{\text{C}} = \frac{P_{2\omega_2-\omega_1}}{P_{\omega_1}} = \frac{I_2(a_2)}{I_0(a_2)} \approx \frac{a_2^2}{8}. \tag{27}$$

At the third order intercept point the IMD/C ratio is equal to 1; hence using the value of a_2 at the intercept we can define the value of modulation index m at the third order intercept as m_{int}. Therefore, the RF input power to the link and output power at the intercept point is calculated as

$$P_{\text{in,int}} = \frac{m_{\text{int}}^2 (I_b - I_{\text{th}})^2 |1 - S_{22L}\Gamma_{\text{Las}}|^2 Z_0}{|S_{21L}|^2 |1 - \Gamma_{\text{Las}}|^2}, \tag{28}$$

and

$$P_{\text{out,int}} = P_{\text{in,int}} \times G. \tag{29}$$

The 1 dB compression point is calculated in a similar fashion. For small input RF powers the output power at the fundamental frequency increases linearly with the input power, since

$$\frac{I_1(a_1)}{I_0(a_1)} = \frac{a_1}{2}\left[\frac{1 + \frac{a_1^2}{8} + \frac{a_1^4}{192}}{1 + \frac{a_1^2}{4} + \frac{a_1^4}{64}}\right] \approx \frac{a_1}{2} \quad \text{for small } a_1. \tag{30}$$

Thus for small input RF powers the power at the fundamental frequency is

$$P_{\omega_1 \text{ linear}} = a_1 P_0 \cos(\omega_1 t + \theta_1). \tag{31}$$

At larger input RF powers the fundamental begins to saturate. This response can be obtained by considering more terms of the modified Bessel functions in the expression for the fundamental, which gives

$$P_{\omega_1 \text{ saturated}} = \frac{a_1}{3}\left[\frac{a_1^4 + 24a_1^2 + 192}{a_1^4 + 16a_1^2 + 64}\right] P_0 \cos(\omega_1 t + \theta_1). \tag{32}$$

The RF power at the output of the link is given by

$$P_{\text{outrf}} = K_L^2 L^2 K_D^2 \eta_D^2 P_{\omega_1}^2 G_{RX} Z_0. \tag{33}$$

The 1 dB compression point is then calculated at the RF input power where the output power diverges from the linear gain by 1 dB, or in a linear form,

$$\frac{P_{\text{out,rf linear}}}{P_{\text{out,rf saturated}}} = \frac{P_{\omega_1 \text{ linear}}^2}{P_{\omega_1 \text{ saturated}}^2} = 1.2589, \tag{34}$$

giving $a_1 = 1.00952$ at the 1 dB compression point. From this value of a_1 we obtain the value of m [16]. On substituting the value of m at the 1 dB compression point in the expression for input RF power we obtain the input power at the 1 dB compression point as

$$P_{\text{in,1 dB CP}} = \frac{m_{\text{1 dB CP}}^2 (I_b - I_{\text{th}})^2 |1 - S_{22L}\Gamma_{\text{Las}}|^2 Z_0}{|S_{21L}|^2 |1 - \Gamma_{\text{Las}}|^2}, \tag{35}$$

and

$$P_{\text{out,1 dB CP}} = \frac{P_{\text{in,1 dB CP}} \times G}{1.2589}. \tag{36}$$

The spurious-free and compression dynamic ranges of the directly modulated FO link are defined as follows:

$$\text{SFDR} = \left(\frac{P_{\text{out,int}}}{N_{\text{out}}}\right)^{2/3}, \tag{37}$$

$$\text{CDR} = \frac{1.2589 \times P_{\text{out,1 dB CP}}}{N_{\text{out}}}. \tag{38}$$

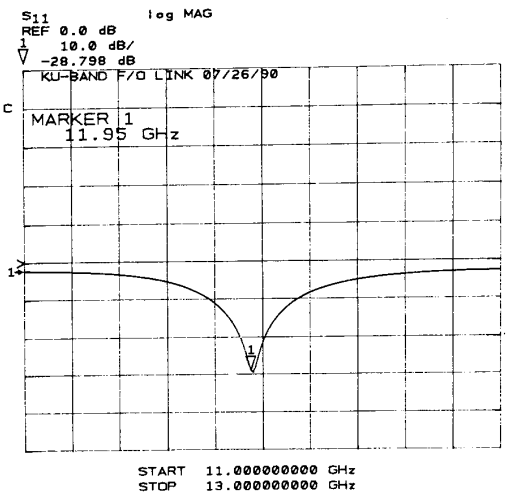

(a)

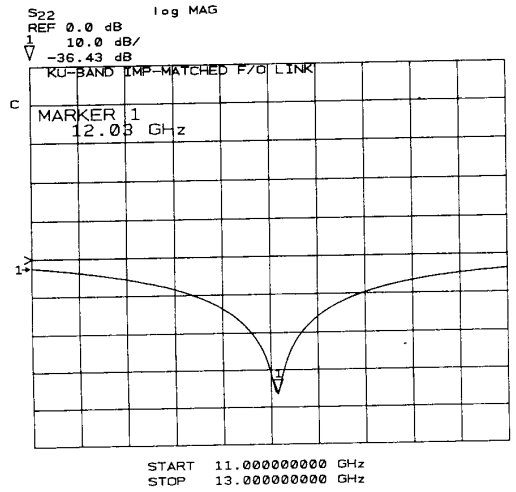

(b)

Fig. 6. Measured input and output return losses of the *Ku*-band (11.6–12.4 GHz) direct modulation fiber optic link, accomplished using single-stage reactive matching networks. (a) Return loss of the impedance-matched laser. (b) Return loss of the impedance-matched detector.

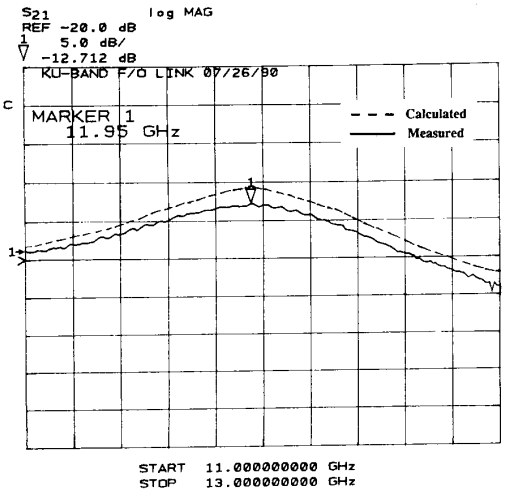

Fig. 7. Insertion loss comparison of the experimental and analytical results of a direct modulation fiber-optic link over the 11–13 GHz frequency range.

Experiments

A direct modulation link was developed for operation at 11.6–12.4 GHz using an InGaAsP distributed-feedback laser diode. This device emits at the 1.3 μm wavelength and features a responsivity of $\eta_L = 0.26$ mW/mA when biased well above its threshold current of 13 mA. The detector used in the link was a single-mode fiber-pigtailed 1.3 μm-wavelength p-i-n photodiode with a responsivity of $\eta_D = 0.56$ mA/mW and a 3-dB modulation bandwidth of 15 GHz. The laser diode and photodetector had been mounted in standard microwave test fixtures to enable de-embedding of the device impedances out of the test fixtures. Based on the de-embedded equivalent circuit model of these devices, the Bode–Fano's theorem [17] predicts for a minimum return loss of 10-dB, reactive matching bandwidths greater than 6 GHz for the laser diode and 4 GHz for the photodetector at center frequency of 12 GHz can be obtained.

Using these devices optical transmitter and receiver modules were fabricated. The reactively matched optical interface modules are shown in Fig. 5, where a single-stage distributed matching network and the single-mode optical fiber coupling are visible in the optical transmitter. Narrowband reactive matching of the optical receiver was accomplished via internal modifications to a commercial photodetector package. The electrical input and outputs are 50 Ω microstrip transitions to SMA connectors. Measured 12 GHz return losses of 29 dB and 36 dB were obtained respectively for the laser and photodetector modules, as shown in Fig. 6, when inductances and capacitances that constitute the matching circuits were properly tweaked.

Optical power was coupled from the laser to the active region of the detector with an efficiency $(K_L \cdot L \cdot K_D)$ of 40% using a plano-convex gradient-index (GRIN) lens with AR-coated facets to focus the diverging output beam of the semiconductor laser into the 8 μm core of the single-mode fiber. This resulted in a link current transfer function $H_L = 0.058$ at 12 GHz. Based on this efficiency and on the equivalent circuit models of the laser and detector modules, the gain of the link was predicted using (8). This predicted gain is plotted as a function of frequency alongside the measured gain in Fig. 7. Both curves have 3-dB bandwidths of ~ 800 MHz and peak at 12 GHz, where the analytically predicted response is -10.9 dB compared to the measured gain of -12.6 dB. The 1.7 dB difference may be accounted for by the discrepancy between the scattering parameters of the simulated

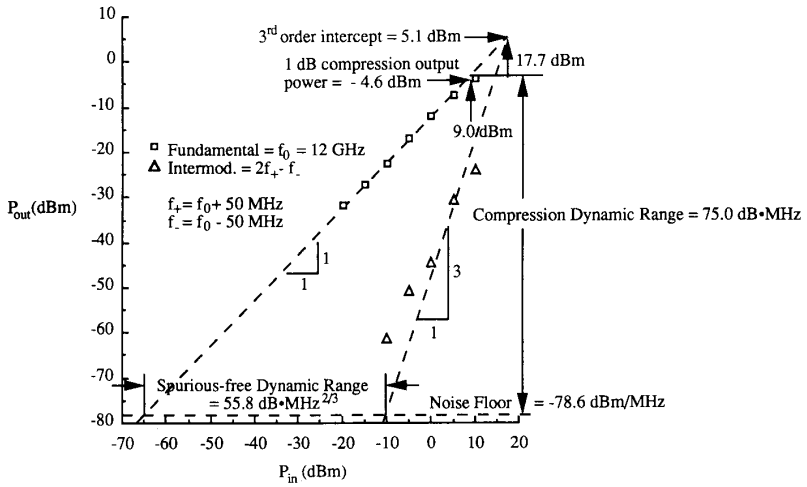

Fig. 8. Measured dynamic range of the experimental direct modulation fiber-optic link at 12 GHz.

matching network and those of the tweaked matching circuits.

Fig. 8 shows the plot of the measured direct modulation link output power versus input RF power of the fundamental and the third order intermodulation product at 12 GHz. It also shows the compression dynamic range and the spurious free dynamic range for the link obtained from measurements. The compression dynamic range is 75.0 dB in a 1 MHz receiver bandwidth, or 135.0 dB·Hz; the spurious free dynamic range is 55.8 db·$MHz^{2/3}$ (95.8 dB·$Hz^{2/3}$). The measured noise floor spectral power density level is -138.6 dBm/Hz. These results compare very favorably with the predicted spurious-free dynamic range of 97.3 dB·$Hz^{2/3}$ and noise floor spectral density of -140.1 dBm/Hz. Discrepancies between the predicted and measured performance parameters is partly due to lack of good data on the tweaked matching circuit and may also be caused in part by a number of phenomena that are difficult to quantify—for instance, the effect of finite optical reflections, such as from the input fiber end face back to the laser, upon laser noise and linearity.

Discussion

The analysis and experimental results show how the gain, noise figure, and dynamic range of the direct modulation fiber-optic link could be improved. Obviously, higher electro-optic conversion efficiencies from the laser and detector would increase the gain, as would improvements in optical coupling efficiencies. Additionally, gain is proportional both to the transducer gain of the laser matching circuit, which is inversely proportional to the laser forward junction resistance, and to that of the photodetector matching circuit, which is inversely related to the reverse junction resistance and capacitance of the pin photodiode. As the desired operating bandwidth of the fiberoptic link is increased, the Q factors of the devices must be lowered according to Bode–Fano's theorem [17], and thus the transducer gains of the laser and detector circuits will degrade, lowering gain that can be achieved.

Linear operation of a direct modulation fiber-optic link also depends largely on the ability to bias the laser diode at low modulation indices and away from the large-signal relaxation oscillation peak, which is dependent on the laser diode structure. To improve the dynamic range of the direct modulation link, laser diodes with lower RIN noise must be developed. For instance, semiconductor laser diode architectures involving the deposition of a reflective coating on the laser's rear facet (asymmetric) have demonstrated lower RIN noise than those with facets of equal reflectivity (symmetric) [16]. If efforts along these lines produce semiconductor lasers with noise approaching the shot-noise imposed low-noise limit, 10 dB lower noise figure and 6–8 dB·$Hz^{2/3}$ broader spurious-free dynamic range may be exhibited by direct modulation fiberoptic links. Approaches to increase the relaxation oscillation frequency of semiconductor lasers, thereby allowing modulation at higher frequencies and reducing the noise at a given frequency below the relaxation oscillation, often involve using distributed feedback structures rather than the Fabry–Perot architecture. Lower noise is ensured, however, only if the laser is shielded from optical feedback using an optical isolator between the laser and reflecting surfaces like the input end face of the optical fiber.

Externally Modulated FO Links

Gain Analysis

The small-signal gain of an externally modulated fiber-optic link is derived using the SFD technique as was applied to direct modulation. When a lumped-element Mach–Zehnder interferometric modulator is employed in the optical transmitter to impress a microwave signal upon the optical carrier, the transmitter SFD is obtained by considering the capacitance C_m across the modulator

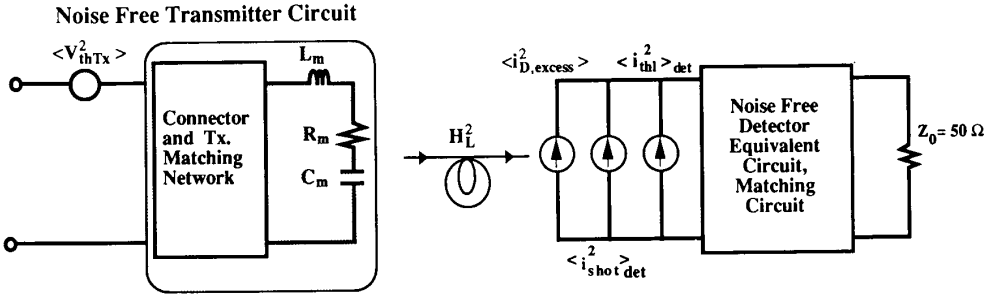

Fig. 9. Schematic representation of noise sources in an externally modulated FO link.

terminals to be the termination load Γ_M of a two-port network (represented by $[S_M]$) consisting of the microwave impedance-matching circuit and the other device parameters in the equivalent circuit of the modulator, Fig. 2(a). Fig. 2(b) shows the SFD for the transmitter in an externally modulated FO link. The output power of a fiber-optic link depends on the amplitude of the detected photocurrent, I_{det}, which is in turn proportional to the RF voltage ν_m across the capacitor C_m. This RF voltage is expressed as

$$\nu_m = \sqrt{Z_0}\,(a_{Lm} + b_{Lm}), \tag{39}$$

where a_{Lm} and b_{Lm} are the square roots of the incident and reflected powers at the modulator terminal capacitance and Z_0 is the characteristic impedance of the input system (50 Ω). From the SFD it is clear that

$$b_{Lm} = a_{Lm}\Gamma_M, \quad \text{and}$$
$$a_{Lm} = \frac{b_{sm}S_{21m}}{1 - S_{22m}\Gamma_M} \quad \text{since } \Gamma_S = \Gamma_{SM} = 0, \tag{40}$$

where b_{sm} is the normalized incident transmitter power. Therefore,

$$|\nu_m| = \sqrt{\frac{Z_0|b_{sm}|^2|S_{21m}|^2|1+\Gamma_M|^2}{|1 - S_{22m}\Gamma_M|^2}}$$
$$= \sqrt{\frac{Z_0 P_{\text{in},Tx}|S_{21m}|^2|1+\Gamma_M|^2}{|1 - S_{22m}\Gamma_M|^2}}, \tag{41}$$

where $P_{\text{in},Tx}$ is the (unnormalized) RF input power to the external modulation link. Based on the $P_{\text{opt}} - V$ curve of the lumped-element interferometric modulator, the optical output of the modulator can be represented in terms of the dc optical input $P_{\text{in,op}}$ as

$$P_{\text{out,op}} = P_{\text{in,op}}\cos^2\left(\frac{\pi}{4} - \frac{\pi V_M}{2V_\pi}\right)$$
$$= \frac{P_{\text{in,op}}}{2}\left(1 + \sin\left(\frac{\pi V_M}{V_\pi}\right)\right), \tag{42}$$

where $V_M = V_b + \nu_m \sin\omega t$, V_π is the bias voltage required for 100% modulation, and V_b is the dc bias applied to the modulator. For small signals the output reduces to

$$P_{\text{out,op}} = P_{\text{in,op}}\left(\frac{\pi\nu_m}{2V_\pi}\right)\cos\left(\frac{\pi V_b}{V_\pi}\right). \tag{43}$$

The detected photocurrent is defined

$$I_{\text{det}} = LK_D\eta_D P_{\text{out,op}}, \tag{44}$$

where L, K_D, and η_D are as defined previously. Therefore, it is clear that

$$|I_{\text{det}}|^2 = \left(LK_D\eta_D\frac{\pi P_{\text{in,op}}}{2V_\pi}\right)^2\cos^2\left(\frac{\pi V_b}{V_\pi}\right)\frac{|S_{21M}|^2|1+\Gamma_M|^2}{|1 - \Gamma_M S_{22M}|^2}$$
$$\cdot Z_0 P_{\text{in},Tx}. \tag{45}$$

Using the expression for G_{Rx} previously derived, the small-signal gain of the external modulation link operated at its linear dc bias voltage is obtained:

$$G = \left(LK_D\eta_D\frac{\pi P_{\text{in,op}}Z_0}{2V_\pi}\right)^2$$
$$\cdot\cos^2\left(\frac{\pi V_b}{V_\pi}\right)\frac{|S_{21M}|^2|S_{21D}|^2|1+\Gamma_M|^2}{|1 - \Gamma_M S_{22M}|^2|1 - \Gamma_{sD}S_{11D}|^2}. \tag{46}$$

Noise Analysis

The noise analysis of the externally modulated link is performed in manner almost identical to that of the directly modulated link. Fig. 9 shows the schematic of the externally modulated link with the noise sources categorized as the transmitter's thermal and excess noise and the receiver's thermal and shot noise.

The transmitter's thermal noise sources are represented as one equivalent thermal noise voltage at the transmitter's input. This noise voltage is then transformed into the noise power at the output of the link, using the gain across the complete link, as

$$N_{\text{thtx}} = 2kT_aB\left(\frac{\pi LK_D\eta_D P_{\text{in,op}}Z_0}{2V_\pi}\right)^2$$
$$\cdot\cos^2\left(\frac{\pi V_b}{V_\pi}\right)\frac{|S_{21m}|^2|S_{21D}|^2|1+\Gamma_M|^2}{|1 - \Gamma_M S_{22m}|^2|1 - \Gamma_{sD}S_{11D}|^2}. \tag{47}$$

The excess noise of the laser warrants some explanation. The $\langle i^2_{D,\text{excess}}\rangle$ term is the excess noise arising from

relaxation oscillations in the optical source, and is deduced from spectral power density measurements of the unmodulated output power of the laser. However it can also be calculated from the manufacturer's quoted RIN which includes the shot noise contribution of the receiver as well. This calculation is given as

$$\mathrm{RIN} = \frac{2eI_{\mathrm{dc}} + \langle i^2_{D,\mathrm{excess}} \rangle}{I^2_{\mathrm{dc}}}, \tag{48}$$

where I_{dc}, the dc-detected photocurrent for the given output power from the modulator, is simply

$$I_{\mathrm{dc}} = \frac{LK_D\eta_D P_{\mathrm{in,op}}}{2}\left(1+\sin\frac{\pi V_b}{V_\pi}\right). \tag{49}$$

From this expression we can find the expression for the excess noise power as

$$N_{\mathrm{excess}} = \left[\frac{LK_D\eta_D P_{\mathrm{in,op}}}{2}\left(1+\sin\frac{\pi V_b}{V_\pi}\right)\mathrm{RIN}(I_b,f) - 2e\right] \times \frac{LK_D\eta_D P_{\mathrm{in,op}}}{2}\left(1+\sin\frac{\pi V_b}{V_\pi}\right) B\frac{|S_{21D}|^2}{|1-\Gamma_{sD}S_{11D}|^2}Z_0. \tag{50}$$

The receiver thermal noise power is given as (12). The shot noise of the detector, including the dark current, I_d, is denoted by a current source at the input of the receiver. This current source is transferred to output by G_{RX} and the output impedance to represent the shot noise power as

$$N_{\mathrm{shot}} = 2e\left[\frac{LK_D\eta_D P_{\mathrm{in,op}}}{2}\left(1+\sin\frac{\pi V_b}{V_\pi}\right) + I_d\right] \cdot B\frac{|S_{21D}|^2}{|1-\Gamma_{sD}S_{11D}|^2}Z_0. \tag{51}$$

The total noise power at the output of the optical detector module is the sum of all these individual noise powers. For actively matched optical detectors, the noise contribution from the amplifier should be incorporated as was presented in the direct modulated case, but this will be omitted here. The noise power at the input to the external modulation link is simply kT_aB. Equation (21) gives the noise figure, with the N_{out} term defined as the sum of (12), (47), (50), and (51).

Distortion Analysis

The distortion characteristics of the external modulation link are analyzed with respect to the modulation index m, which for a Mach–Zehnder modulator at a dc bias point V_b is defined as

$$m = \frac{\nu_m}{\frac{V_\pi}{2} - |V_b|} = \frac{2\nu_m}{V_\pi - 2|V_b|}. \tag{52}$$

By letting $V_M = V_b + \nu_m(\sin\omega_1 t + \sin\omega_2 t)$ and substituting into (42), an expression is obtained for the optical power at fundamental frequency:

$$P_{\omega_1} = P_{\mathrm{in,op}}J_0(a)J_1(a)\cos\frac{\pi V_b}{V_\pi}\sin\omega_1 t, \tag{53}$$

and at the frequency of one of the third-order intermodulation products:

$$P_{2\omega_2-\omega_1} = P_{\mathrm{in,op}}J_1(a)J_2(a)\cos\frac{\pi V_b}{V_\pi}\sin(2\omega_2-\omega_1)t, \tag{54}$$

where we have defined $a = \pi\nu_m / V_\pi$. Therefore, the ratio of third-order intermodulation product output power to that of the fundamental is dependent only on the small-signal modulation voltage ν_m and not upon the dc bias level V_b. Specifically,

$$\frac{\mathrm{IMD}}{\mathrm{C}} = \frac{P_{2\omega_2-\omega_1}}{P_{\omega_1}} = \frac{J_2(a)}{J_0(a)} \tag{55}$$

Given the Taylor series expansions of the 0th and 2nd order Bessel functions:

$$J_0(a) = 1 - \frac{a^2}{4} + \frac{a^4}{64} - \cdots \tag{56}$$

$$J_2(a) = \frac{a^2}{8}\left(1 - \frac{a^2}{12} + \frac{a^4}{384} - \cdots\right), \tag{57}$$

we find that for small signals

$$\frac{\mathrm{IMD}}{\mathrm{C}} \cong \frac{a^2}{8} = \frac{1}{8}\left(\frac{\pi\nu_m}{V_\pi}\right)^2 = \frac{\pi^2 m^2}{32}\left(1 - \frac{2|V_b|}{V_\pi}\right)^2. \tag{58}$$

The small-signal behavior of the fundamental and third-order intermodulation product is extrapolated to determine the modulation index at the third-order intercept—i.e., where IMD/C = 1:

$$m_{\mathrm{int}} = \frac{\sqrt{32}}{\pi\left(1 - \frac{2|V_b|}{V_\pi}\right)}. \tag{59}$$

By expressing the RF input power to the link in terms of the modulation index m rather than modulation voltage ν_m and substituting $m = m_{\mathrm{int}}$, we obtain the input power at the third order intercept as

$$P_{\mathrm{in,int}} = \frac{m^2_{\mathrm{int}}(V_\pi - 2|V_b|)^2|1 - S_{22m}\Gamma_M|^2}{4Z_0|S_{21m}|^2|1+\Gamma_M|^2}. \tag{60}$$

and

$$P_{\mathrm{out,int}} = P_{\mathrm{in,int}} \times G, \tag{61}$$

where G is the gain. For small input RF powers the output power at the fundamental frequency increases

linearly with the input power, since

$$J_1(a)J_0(a) = \frac{a}{2}\left(1-\frac{a^2}{8}+\frac{a^4}{192}-\cdots\right)\left(1-\frac{a^2}{4}+\frac{a^4}{64}-\cdots\right) \approx \frac{a}{2} \text{ for small } a. \quad (62)$$

At larger input RF powers the fundamental begins to saturate. This response is obtained by considering more terms of the Bessel function. Compression of the fundamental output power by 1 dB means that

$$\frac{P_{\text{out,rf linear}}}{P_{\text{out,rf saturated}}} = \frac{P^2_{\omega_1 \text{ linear}}}{P^2_{\omega_1 \text{ saturated}}} = 1.2589, \quad (63)$$

where $P_{\omega 1}$ is given by (53). Therefore, 1 dB of AM compression occurs when

$$\frac{\frac{a^2}{4}}{\left(1-\frac{a^2}{4}+\frac{a^4}{64}-\cdots\right)^2 \frac{a^2}{4}\left(1-\frac{a^2}{8}+\frac{a^4}{192}-\cdots\right)^2} = 1.2589, \quad (64)$$

which corresponds to $a = 0.5500$. From this value of $a = (\pi v_m / V_\pi)$, (52) is used to obtain the value of the modulation index m at the point of 1 dB compression. Substituting this into the equation for input RF power in terms of modulation index m, the input power at the 1 dB compression point is

$$P_{\text{in,1 dB }CP} = \frac{(0.5500)^2 V_\pi^2 |1 - S_{22m}\Gamma_M|^2}{\pi^2 Z_0 |S_{21m}|^2 |1+\Gamma_M|^2}, \quad (65)$$

$$P_{\text{out,1 dB }CP} = \frac{P_{\text{in,1 dB }CP} \times G}{1.2589}. \quad (66)$$

The spurious-free and compression dynamic ranges of the external modulation link are defined exactly as they are for the direct modulation link, i.e.:

$$\text{SFDR} = \left(\frac{P_{\text{out,int}}}{N_{\text{out}}}\right)^{2/3}, \quad (67)$$

$$\text{CDR} = \frac{1.2589 \times P_{\text{out,1 dB }CP}}{N_{\text{out}}}. \quad (68)$$

Experiments

An externally modulated FO link was developed at 875–925 MHz to examine the validity of the analytical model. A 1.3 μm $LiNbO_3$ Mach–Zehnder interferometric modulator with a lumped-element electrode structure was selected. The device exhibited a 23 dB extinction ratio when TE-polarized light was launched into its polarization-preserving input single-mode fiber pigtail. In addition, a switching voltage $V_\pi = 8.3$ V and a 3-dB modulation bandwidth of 3 GHz were quoted by the manufacturer. An InGaAs p-i-n photodiode with a responsivity

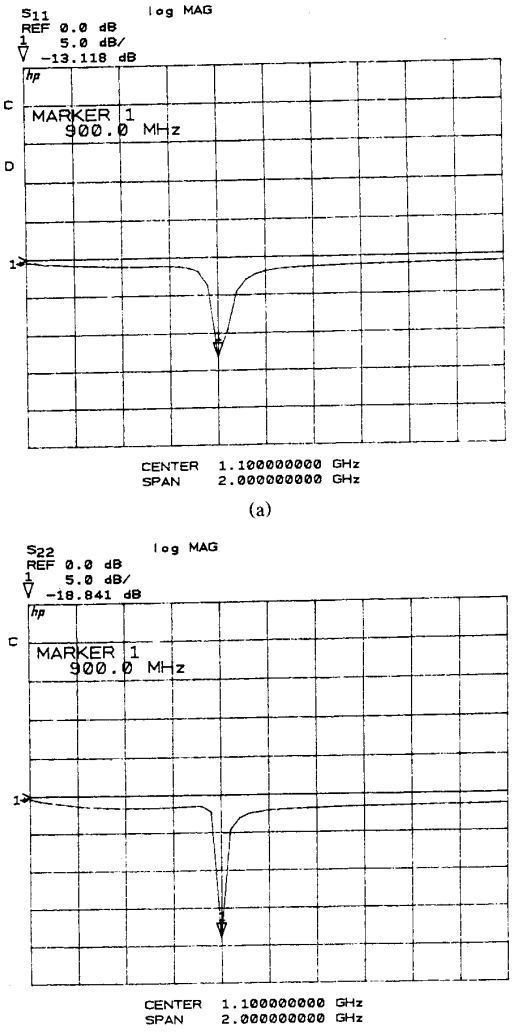

Fig. 10. Measured input and output return losses of the L-band (875–925 MHz) external modulation fiber-optic link, accomplished using single-stage reactive matching networks. (a) Return loss of the impedance-matched modulator. (b) Return loss of the impedance-matched detector.

$\eta_D = 1.0$ mA/mW and frequency response bandwidth of 10 GHz was employed in the optical receiver.

Using the scattering parameters of the modulator and photodetector, de-embedded from the measured S-parameters, equivalent circuit models were developed by fitting them to the measured impedance. This made possible the design and construction of single-stage reactive circuits to impedance-match the electro-optic devices to 50 Ω at the link design frequency of 900 MHz. Based on the external Q-factors of these devices, Bode–Fano's theorem predicts that for 10-dB minimum return loss at the center frequency of 900 MHz, reactive matching bandwidths of only 115 MHz for the lumped-element

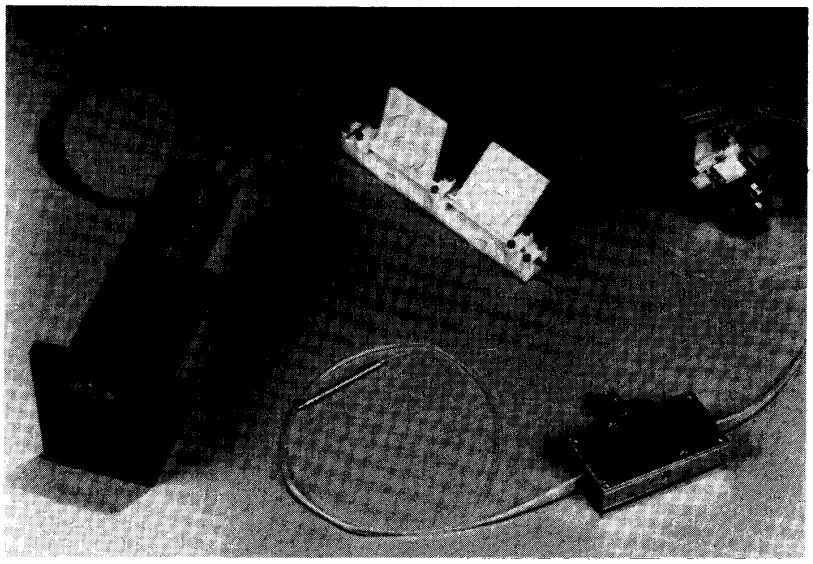

Fig. 11. Experimental L-band external modulation fiber-optic link consisting of (left to right) a high-power (60 mW) single-mode fiber-pigtailed solid-state laser, optical polarization controller, and impedance-matched modulator and detector modules.

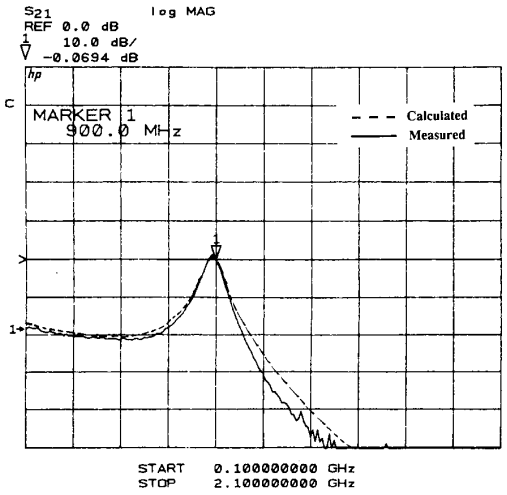

Fig. 12. Insertion loss comparison of the experimental and analytical results of an external modulation fiberoptic link over the 0.1–2.1 GHz frequency range.

modulator and 60 MHz for the reverse-biased photodetector can be obtained. Measured input and output 900 MHz return losses of 13 dB and 18 dB were obtained (Fig. 10) when matching circuits were constructed and properly tweaked. In the figure, actual -10 dB return loss bandwidths of 50 MHz for the input and 40 MHz for the output are apparent.

In order to maximize the gain and dynamic range of the external modulation like, large optical pump power—60 mW at $\lambda = 1.3$ μm—was obtained from a single-mode fiber-pigtailed Nd:YAG laser source. The solid-state laser and the optical receiver were optically coupled to the modulator's input and output fibers, respectively, and the input optical polarization was adjusted to maximize the ratio of optical power measured at the "ON" and "OFF" state switch voltages. The photograph of the externally modulated FO link consisting of the solid-state laser, polarization control device, and reactively matched 900 MHz modulator and photodetector modules, is shown in Fig. 11.

At the modulator's linear, half-power bias point, a dc photodetected current $I_{dc} = (LK_D\eta_D P_{in,op})/2 = 4.3$ mA was measured. Based on this measurement and on the scattering parameters derived from the equivalent circuit model of the externally modulated FO link, (46) was used to predict the small-signal gain for the frequency range of 0.1–2.1 GHz. This calculated result is plotted as a function of frequency in Fig. 12 along with the measured gain. Especially at the design frequency of 900 MHz where both peak at the gain of 0 dB, the agreement between the predicted and measured gain curves is excellent. Both curves show a 3-dB link bandwidth of approximately 50 MHz.

A two-tone intermodulation distortion measurement was performed to determine the spurious-free and compression dynamic ranges of the external modulation fiber-optic link at its center frequency of 900 MHz. Fig. 13 shows the results of the intermodulation distortion measurement as well as the measured output noise floor of the link. The thermal noise of the modulator and detector and the dark current and short noise power were calculated using (12), (47), and (51), and the excess noise was determined by subtracting the sum of these noise powers from the measured total noise floor $P_{N,out}$. A noise figure of 24.3 dB was measured at 900 MHz. As shown, the measured 1 dB compression and third-order

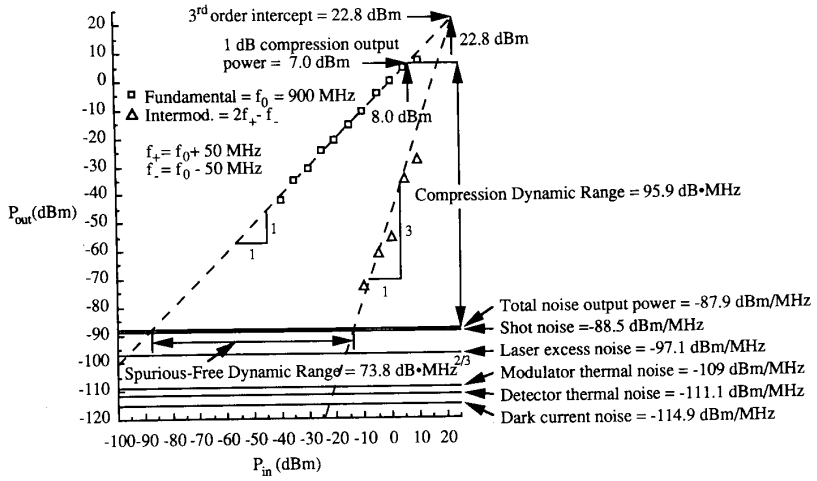

Fig. 13. Results of a two-tone intermodulation distortion measurement, showing the 1 dB compression and third order intercept points of the external modulation link at 900 MHz. Also plotted are the calculated noise powers contributing to the measured output noise floor in a 1 MHz bandwidth. The link's 95.9 dB·MHz compression dynamic range and spurious-free dynamic range of 73.8 dB·MHz$^{2/3}$ are rendered as well.

intercept output powers are 7 dBm and 22.8 dBm, respectively. Thus, the compression dynamic range under these conditions is 95.9 dB·MHz (155.9 dB·Hz) and the spurious-free dynamic range is 73.8 dB·MHz$^{2/3}$ (113.8 dB·Hz$^{2/3}$), the largest dynamic range reported to date for any microwave fiber-optic link. These results very closely match the predicted noise figure and spurious-free dynamic range values of 24.1 dB and 112.7 dB·Hz$^{2/3}$. It was observed that the measured *P-V* curve of the modulator deviated from perfect sinusoidal behavior, which may have created some discrepancy between predicted and measured performance parameters since Bessel functions cannot accurately predict the 1 dB compression and third-order intercept points in such an instance.

Discussion

This analytical model clearly indicates that the available optical source power must be maximized to improve the external modulation link performance. Not only is the link gain proportional to $P_{\text{in,op}}^2$, but since the shot noise dominates over the RIN of the solid-state laser the noise floor increases proportional only to $P_{\text{in,op}}$. Therefore, if very high optical power can be attained without saturating the modulator, the external modulation link will approach its noise figure limit of 3 dB. This amounts to a 21 dB improvement in noise figure, and consequently a 14 dB·Hz$^{2/3}$ improvement in spurious-free dynamic range over the results presented here.

The ability of the detector to handle a large reverse bias and high incident optical powers is necessary before the external modulation link noise figure can approach its thermal noise limit of 3 dB, which would maximize the link's dynamic range. Detector design may be even more critical in the external modulation link than in the direct modulation link since modulation of very high optical power remains linear up to high RF powers which may saturate the photodetector.

Conclusion

Complete analytical models of direct and external modulation fiberoptic link performance have been presented and experimentally verified. Consequently, the potential for very high gain and wide dynamic range has been demonstrated by the analytical approach, especially in the case of the external modulation link with the Nd:YAG laser as its optical source. An experimental *Ku*-band (11.6–12.4 GHz) fiber-optic link was designed and constructed using the direct modulation link models, and featured a minimum insertion loss of −12.6 dB at 12 GHz and a spurious-free dynamic range of 95.8 dB·Hz$^{2/3}$. An experimental *L*-band (875–925 MHz) fiber-optic link designed using the external modulation models exhibited a peak RF insertion gain of 0 dB and compression and spurious-free dynamic ranges of 155.9 dB·Hz and 113.8 dB·Hz$^{2/3}$, respectively.

The analytical models not only allow for a pre-design comparison of link architectures to achieve a given level of performance, but also specify what must be done in order to improve any given performance parameter. The equations predicting the various performance parameters are functions of the laser dc bias current in the case of direct modulation and modulator dc bias voltage in the case of external modulation. In this paper results were reported and discussed at the bias settings at which the RF insertion gain of each link was maximum. The dependence of the performance parameters upon the bias conditions is more complex in both the direct and external modulation scenarios, and this expansive subject is reported elsewhere [15], [16], and [18].

REFERENCES

[1] P. R. Herczfeld, Guest Ed., *IEEE Trans. Microwave Theory Tech.*, Special Issue, vol. 38, no. 5, May 1990.

[2] D. Polifko and A. S. Daryoush, "Comparison of two architectures for fiber-optic distribution inside Ka-band communication satellites," in *1991 MTT-S Int. Microwave Symp. Dig.*, Boston, MA, June 1991.

[3] R. Saedi, X. Zhou, A. S. Daryoush, P. R. Herczfeld, and B. Even-Or, "Recirculating fiberoptic link for memory loop," in *1991 MTT-S Int. Microwave Symp. Dig.*, Boston, MA, June 1991.

[4] A. Paolella, P. R. Herczfeld, A. Madjar, and T. Higgins, "Optical response of the GaAs MESFET at microwave frequencies and applications," in *1991 MTT-S Int. Microwave Symp. Dig.*, Boston, MA, June 1991.

[5] G. E. Betts, L. M. Johnson, C. H. Cox III, and S. D. Lowney, "High-performance optical analog link using external modulator," *IEEE Photon. Technol. Lett.*, vol. 1, no. 11, Nov. 1989.

[6] S. Wang and S. Lin, "High speed III-V electrooptic waveguide modulators at $\lambda = 1.3$ μm," *J. Lightwave Technol.*, pp. 165–171, Feb. 1988.

[7] W. E. Stephens and T. Joseph, "System characteristics of direct modulated and externally modulated RF fiber optic links," *J. Lightwave Technol.*, vol. 5, no. 3, pp. 380–387, Mar. 1987.

[8] M. de La Chappelle, "Computer-aided analysis and design of microwave fiber-optic links," *Microwave J.*, no. 9, pp. 179–186, Sept. 1989.

[9] C. Cox, L. Johnson, and G. Betts, "A theoretical and experimental comparison of directly and externally modulated fiber optic links," *1989 MTT-S Int. Microwave Symp. Dig.*, Long Beach, CA, June 1989.

[10] A. S. Daryoush, E. Ackerman, R. Saedi, R. Kunath, K. Shaulkhauser, "High-speed fiberoptic links for satellite traffic," *IEEE Trans. Microwave Theory Tech.*, vol. 38, no. 5, pp. 510–517, May 1990.

[11] E. Ackerman, D. Kasemset, S. Wanuga, D. Hogue and J. Komiak, "A high gain directly modulated L-band microwave optical link," *1990 MTT-S Int. Microwave Symp. Dig.*, June 1990, Dallas, TX.

[12] A. Papoulis, *Probability, Random Variables, and Stochastic Processes.* New York: McGraw-Hill, 1965.

[13] P. Hill, R. Olshansky, J. Schlafer, and W. Powazinik, "Reduction of relative intensity noise in 1.3 mm InGaAsP semiconductor lasers," *Appl. Phys. Lett.*, vol. 50, no. 20, pp. 1400–1402, May 1987.

[14] J. Hausner, W. Richter, P. Russer, and B. Scheuvens, "A Low Noise Hybrid Integrated 4.5 GBIT/s Optical Front End," in *Proc. 20th European Microwave Conf.*, Budapest, Hungary, vol. 1, Sept. 1990.

[15] S. Iyer, "Study of asymmetric laser diodes under large-signal modulation," M.S. thesis, Drexel University, Philadelphia, PA June 1988.

[16] Tsang-Der Ni, "Non-linear characteristics of symmetric and asymmetric laser diodes," M.S. thesis, Drexel University, Philadelphia, PA, Nov. 1989.

[17] R. M. Fano, "Theoretical limitations on the broadband matching of arbitrary impedances," *J. Franklin Inst.*, vol. 249, Jan.-Feb. 1950, pp. 57–84 and 139–154.

[18] E. Ackerman, D. Kasemset, and S. Wanuga, "External modulation L-band link with 117 dB spurious-free dynamic range," *Microwave J.*, vol. 34, no. 9.

Afshin S. Daryoush (S'84–M'86–SM'91) was born in Iran in 1957. He received the B.S. degree in electrical engineering in 1981 from Case Western Reserve University, Cleveland, OH. He then received the M.S. degree in 1984 and the Ph.D. degree in 1986 from Drexel University, Philadelphia, PA, also in electrical engineering.

After graduation he joined the staff of Drexel University, first as Research Assistant Professor and then, beginning in 1987, as DuPont Assistant Professor of Electrical and Computer Engineering. In 1989 he was promoted to Associate Professor. He has conducted research in the area of optically controlled microwave devices and subsystems, high-speed fiber-optic links, and system studies of large-aperture phased array antennas. During the summers of 1987 and 1988, he was a Summer Faculty Fellow at NASA, Lewis Research Center, Cleveland, OH, conducting research on high-speed fiber-optic links for ACTS project. In the summers of 1989 and 1990 as a Summer Faculty Fellow, he conducted research on high-speed LED for 1.25 Gb/s fiber-optic links for computer backplanes at the Naval Air Development Center, Warminster, PA.

Dr. Daryoush has authored or coauthored over 90 technical publications in the areas of light interaction with passive and active microwave devices, circuits, and systems. He has lectured frequently at workshops and international symposia. The recipient of the Microwave Prize from the 16th European Microwave Conference, Dublin, Ireland, he also received the best paper award at the IMPATT Session of the 1986 International Microwave Symposium, Baltimore, MD. He has also been awarded a U.S. patent on the optically controlled patch antenna. He is a member of Sigma Xi.

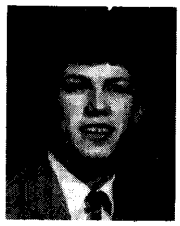

Edward Ackerman (S'86–S'87–M'87–M'89) received the B.S. degree in electrical engineering from Lafayette College, Easton, PA, and the M.S. degree in electrical engineering from Drexel University, Philadelphia, PA. He is currently pursuing the Ph.D. degree at Drexel University.

He is employed as a Microwave Engineer at GE Electronics Laboratory, Syracuse, NY, where he is developing high-fidelity photonic systems for microwave and millimeter-wave communications applications.

Niranjan R. Samant (S'90) was born in Bombay, India in 1968. He received his B.E. degree in electronics and communications engineering from the Mangalore University, India. He is currently working toward the M.S. degree in electrical engineering at Drexel University, Philadelphia, PA. His research interests include design and analysis of fiber optic links.

He is a member of the IEEE Microwave Theory and Techniques Society.

Stephen Wanuga (S'58–M'60–SM'85) received the B.S.E.E. degree from Pennsylvania State University in 1959 and the M.S.E.E. from Syracuse University in 1967.

He is with the General Electric Electronics Laboratory, Syracuse, NY, where he has been responsible for development of various solid state acoustic, microwave and optoelectronic devices and components. Currently he is Project Leader on research and development of broadband low loss microwave photonic links and components for phased array radar and communication systems.

Dumrong Kasemset (M'82) received the S.B., S.M., and Ph.D. degrees from the Massachusetts Institute of Technology, Cambridge, all in electrical engineering, in 1977, 1979, and 1981, respectively.

Since 1989, he has been at GE's Electronics Laboratory, Syracuse, NY, where he has been responsible for developing applications of microwave and digital photonics for GE Aerospace. Currently, he is Manager of Integrated Optoelectronics Programs at GE Electronics Laboratory.